Cite This: *Ind. Eng. Chem. Res.* XXXX, XXX, XXX–XXX

Solketal Production from Glycerol Ketalization with Acetone: Catalyst Selection and Thermodynamic and Kinetic Reaction Study

Miguel N. Moreira, Rui P. V. Faria,* Ana M. Ribeiro, and Alírio E. Rodrigues

Laboratory of Separation and Reaction Engineering—Laboratory of Catalysis and Materials (LSRE-LCM), Department of Chemical Engineering, Faculty of Engineering, University of Porto, Rua Dr. Roberto Frias s/n, 4200-465 Porto, Portugal

S *Supporting Information*

ABSTRACT: In this work, the main results of a thermodynamic and kinetic study of glycerol ketalization to produce solketal in the presence of a solvent are presented. A catalyst and a solvent screening was carried out leading to the selection of Amberlyst-35 ion-exchange resin and ethanol as the most suitable materials for this reaction. A parametric study allowed one to determine reaction equilibrium and kinetic parameters in a batch reactor in the absence of external mass-transfer limitations. Regarding reaction thermodynamic equilibrium, a standard enthalpy of -20.1 ± 1.1 kJ mol^{-1} and a Gibbs free energy of 1.4 ± 0.3 kJ mol^{-1} were obtained. Reaction kinetics was studied assuming different reaction rate laws to fit the experimental data obtained: Pseudo-Homogeneous (PH), Langmuir−Hinshelwood−Hougen−Watson (LHHW), and Eley−Rideal (ER). The experimental results revealed that the reaction kinetics behavior could be accurately described by the LHHW reaction rate law, considering the presence of internal mass-transfer resistances. The activation energy for the overall reaction was found to be 69.0 ± 6.6 kJ mol^{-1}.
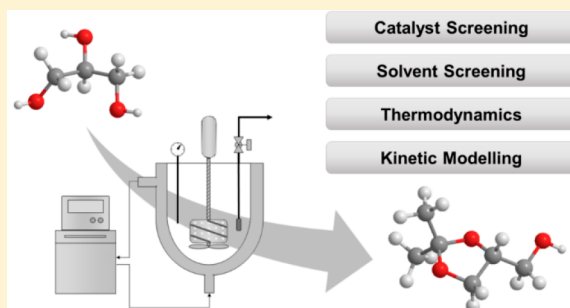
1. INTRODUCTION

The depletion of fossil-based fuels is leading to an increasing demand in the search for alternative fuels, such as biodiesel.[1] Biodiesel derives from biological sources, for example, animal fats and vegetable oils,[2,3] resulting in a sustainable and renewable fuel.

Biodiesel is mainly produced by a transesterification reaction using the raw materials mentioned above,[4,5] which can later be used directly or mixed with a fossil fuel. Glycerol is obtained as the main byproduct from this process. Therefore, in order to solve one problem, another is formed. The continued production of biodiesel led to a continued production of glycerol, and an excessive amount of this byproduct is being left to accumulate. The global production of glycerol in 2020 is expected to reach 5.2 million tons. This is resulting in a continued decrease of glycerol prices, compromising the sustainability and the economy of the biodiesel industry.[6] The current price of crude glycerol is 0.85 €/kg.[7]

Glycerol can be produced from different sources and activities. In Europe, glycerol is mostly formed from animal tallow and vegetable oil. Regarding the United States of America, biodiesel refinery activities are the main source of glycerol production. In Asia, glycerol originates mainly from vegetable oil. For instance, in Malaysia and Indonesia, palm oil is the principal source of glycerol, and in the Philippines, it is coconut oil. Market research has shown that the Asian continent is the largest glycerol producer in the world.[8]

Also, glycerol is not suitable for use as a direct fuel component, once its heating value is low, due to the presence of three hydroxyl groups in the molecule. That being said, new forms of this compound must be developed for its valorization.

There are several value-added applications to transform glycerol into other chemical commodities, such as hydrogen,[9−17] methanol,[18−21] ethanol,[9,22−25] and fuel additives.[26−35]

When the production of fuel additives is considered as the valorization route, through a ketalization reaction with acetone, it is possible to convert glycerol into solketal (4-hydroxymethyl-2,2-dimethyl-1,3-dioxolane). Solketal is useful as an oxygenated fuel additive, since it is capable of reducing particle emission and gum formation in gasoline, can improve the liquid properties for low temperature fuel transportation, and can optimize the octane number when blended with gasoline.[36,37]

The ketalization of glycerol using acetone leads to the formation of two ketal species, one which has a five membered ring and another with a six membered ring. Nevertheless, the six membered ring species is much less favorable since one of the methyl groups is in the axial position of the chair conformation,[34] as shown in Figure 1.

From the above-mentioned ketalization reaction, Vol'eva et al.[38] obtained a molar ratio of about 9:1 between the five membered ring (4-hydroxymethyl-2,2-dimethyl-1,3-dioxolane or solketal) and the six membered ring (5-hydroxy-2,2-
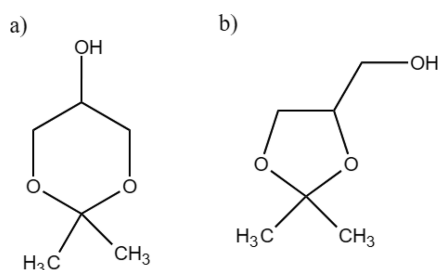
Figure 1. Ketal species resulting from the glycerol ketalization with acetone: (a) 5-hydroxy-2,2-dimethyl-1,3-dioxane; (b) 4-hydroxymethyl-2,2-dimethyl-1,3-dioxolane.

dimethyl-1,3-dioxane), respectively. One possible explanation for this phenomena can be related to the glycerol molecular geometry. It is much more likely that the reaction between acetone and glycerol occurs in a glycerol end-chain hydroxyl group than in the middle-chain hydroxyl group. More recently, Nanda et al.[34] reported a molar ratio of about 99:1 between

the five membered ring and the six membered ring. On the basis of these results, the last species will not be considered in the present work.

Nanda et al.[34] proposed a reaction mechanism, represented in Figure 2. In step 1, in the presence of an acid catalyst, acetone protonates the catalyst surface. This leads almost instantly to a positive pole in the middle carbon of the acetone molecule. In step 2, there is a surface reaction between the adsorbed species and glycerol. The interaction occurs with an end-chain hydroxyl group (primary hydroxyl group) of the glycerol molecule, resulting in an adsorbed hemiacetal. In step 3, water is formed. This is considered to be the rate limiting step. Finally, in step 4, the short-lived carbenium ion leads to the closing of the five membered ring through one of the nonbonding electron pairs of the oxygen atom from the adsorbed ketone, forming the solketal molecule.

The literature reports several catalysts used for ketalizations. Table 1 compiles a literature review of the most active catalysts for solketal production, with a focus on zeolites and ion
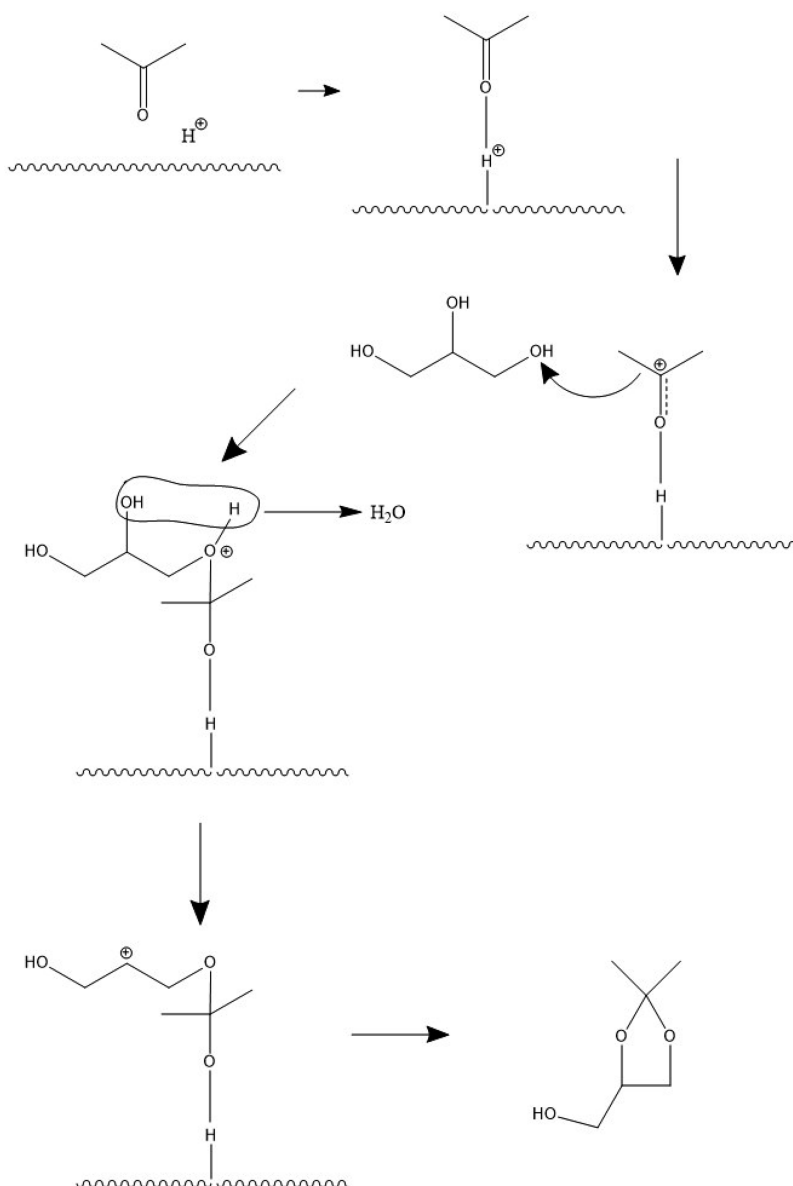

Figure 2. Possible ketalization reaction mechanism for the production of solketal from glycerol and acetone.

Table 1. Catalyst Screening for the Ketalization of Glycerol to Produce Solketal

	catalyst	glyc./acet. molar ratio	temperature (K)	reaction time (h)	lim. react. conv. (%)	ref.
zeolites	zeolite beta (H$^+$)	1:2−1:3	room temp.	2	62−86	39
	ZSM-5 (H$^+$)	1:3	343	1	93	40
	zeolite beta (H$^+$) (Zeolyst CP814E)	1:2−1:6	308	4	60−82	41
	zeolite beta (H$^+$) (Zeolyst CP811T1)	1:2−1:6	308	4	62−85	41
	zeolite HY	1:2−1:6	308	4	21−37	41
	montmorillonite K10	1:6	313	0.25	68	42
ion exchange resins	Amberlyst-15	1:2	343	1	95	43
	Amberlyst-35	1.5:1−2.5:1	298−318	8	60−74	44
	Amberlyst-36	1:1.5	313	8	88	45
	Lewatit GF101	1:3−1:12	303−313	4	34−96	46
	Purolite CT275DR	1:4	313	6	43	46
	Purolite CT276	1:4	313	6	36	46

exchange resins that have revealed a particularly high catalytic activity for this reaction.

The miscibility between acetone and glycerol is poor[47] and, for that reason, few authors suggest adding a solvent to overcome this issue. Despite that fact, the synthesis of solketal has been carried out with relative success in different types of reactors, from batch reactors to packed reactors, reactive distillation, or membrane reactors.[34]

In this work, instead of limiting the research to the development of a new catalyst or to the optimization of the reaction conditions for the synthesis of solketal, an extensive study of glycerol ketalization with acetone was carried out using commercially available catalysts in order to set the basis for the development of glycerol valorization processes, through its conversion into solketal, with particular attention to sorption-enhanced reactive processes, reported as one of the most promising strategies for this kind of system.[48] In the first stage, a solvent selection methodology specifically designed for this purpose was applied.[49] Once the solvent was selected, fundamental data was collected aiming to determine the dependence of the chemical equilibrium constant on the temperature and to estimate the reaction standard Gibbs free energy, ΔG^0, and standard enthalpy, ΔH^0, considering a nonideal liquid-phase model determining the activity of each species through the UNIFAC group contribution method. The description of the nonideality of a mixture is fundamental for the development of more complex processes as multifunctional reactors, such as reactive distillation, membrane reactor, and chromatographic reactors, among other processes and has been neglected in the majority of the previously reported works regarding the synthesis of solketal.

The reaction kinetics study started with a catalyst screening, focused on acid ion-exchange resins and zeolites. Once the most suitable catalyst had been selected, the effect of several variables on the reaction rate was experimentally evaluated in order to determine a model that accurately describes the reaction kinetics over a wide range of operating conditions. Three reaction rate laws were considered, namely, Langmuir−Hinshelwood−Hougen−Watson, Pseudo-Homogeneous, and Eley−Rideal models. The influence of the internal mass-transfer limitations, the amount of eluent, and the nonideality of the system in the synthesis of solketal was also considered in the present work, in opposition to prior studies.

2. EXPERIMENTAL SECTION

2.1. Chemicals and Catalyst.
The chemicals used in the experimental tests were ethanol (>99%) purchased from

Panreac-AppliChem, dimethyl sulfoxide (>99%) purchased from VWR International, glycerol (>99%) purchased from Sigma-Aldrich, and acetone (>99%) purchased from Fisher Chemicals.

Rohm and Haas Amberlyst-15 and Amberlyst-35 ion exchange resins were used as catalysts. Water adsorbs strongly on Amberlyst-15 and Amberlyst-35, and it can lead to a decrease of the reaction rate, since it is a product of the reaction; therefore, predried resin must be used on the reaction tests. For that purpose, the resin was washed several times with deionized water; then, it was washed with ethanol and dried at 333 K. Süd-chemie H-BEA25 zeolite was also tested. Before using it, the zeolite was calcined at 593 K overnight. Table 2 presents the most relevant physical properties of the catalyst used.[44,50−52]

Table 2. Amberlyst-15, Amberlyst-35, and Zeolite H-BEA 25 Physical Properties

	Amberlyst-15	Amberlyst-35	Zeolite H-BEA 25
acidity (eq·kg^{-1})	4.7	5.2	NA
SiO$_2$/Al$_2$O$_3$ (mol/mol)	NA	NA	25:75
average pore diameter (nm)	30	30	0.51
max operating temp (°C)	120	150	NA
pore volume (mL·g^{-1})	0.400	0.425	0.748
BET surface area (m^2·g^{-1})	53	50	452
apparent density (kg·m^{-3})	771	931	924

2.2. Analytical Method.
The samples collected at predefined time intervals during the experiments performed were analyzed in a gas chromatograph (DANI Master GC), using dimethyl sulfoxide as the internal standard. Helium was used as the carrier gas at a flow rate of 4.90 mL·min^{-1}. The separation of the compounds was carried out in a ParaBondQ column (25 m, 0.53 mm i.d., film thickness of 10.0 μm) and quantified by a thermal conductivity detector. The linear velocity was set to 40 cm·s^{-1}, and the injection volume used was 2 μL with a split of 10. The temperatures of the injector and thermal conductivity detector were set to 573.15 K. The initial column temperature was 423.15 K, followed immediately by a temperature increase at 5 K·min^{-1} until 553.15 K and subsequently held constant for 1 min. Each of the samples collected during the experiments performed in this work was analyzed in triplicate to evaluate the reproducibility of the conversion determined values.
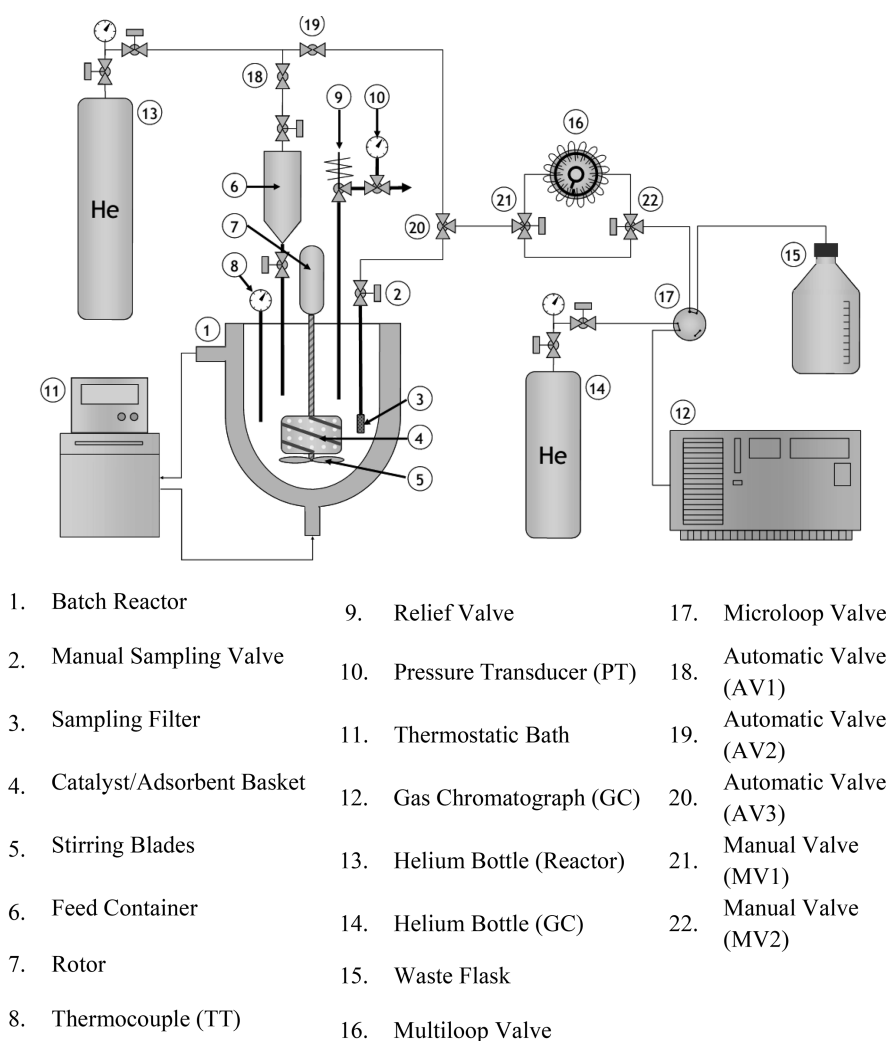
Figure 3. Schematic representation of the batch reactor and all its adjacent equipment.

1. Batch Reactor
2. Manual Sampling Valve
3. Sampling Filter
4. Catalyst/Adsorbent Basket
5. Stirring Blades
6. Feed Container
7. Rotor
8. Thermocouple (TT)
9. Relief Valve
10. Pressure Transducer (PT)
11. Thermostatic Bath
12. Gas Chromatograph (GC)
13. Helium Bottle (Reactor)
14. Helium Bottle (GC)
15. Waste Flask
16. Multiloop Valve
17. Microloop Valve
18. Automatic Valve (AV1)
19. Automatic Valve (AV2)
20. Automatic Valve (AV3)
21. Manual Valve (MV1)
22. Manual Valve (MV2)

2.3. Experimental Tests for Catalyst and Solvent Selection. The solvent selection methodology applied in the present work comprises a stage in which the solvents that evidence the highest potential in a preliminary theoretical screening are tested to assess their impact in the reaction kinetics and in the reaction products adsorption. In this work, the procedure was adapted so that the catalyst and solvent screening could be performed simultaneously. For that purpose, batch reactions were carried out in 50 mL glass vessels. A benchtop incubator shaker SI-300R from Lab. Companion was used to supply heat and to stir the reaction mixtures composed by the stoichiometric ratio of 1:1 of acetone and glycerol diluted in 50% of solvent (molar basis). The reactor was loaded with 1.0 wt % of catalyst considering the total mass of the system (i.e., mass of reactants plus mass of solvent). The experiments were carried out for 24 h at 313 K. Additionally, adsorption tests were carried out in a fixed bed column packed with the catalysts previously selected and using as eluent the solvents from the screening methodology applied, at a flow rate of 2 mL/min, temperature of 313 K, and injecting a 200 μL loop containing solketal and water (pure). Through the average residence times computed from the outlet concentration histories of each experiment, it was possible to evaluate the effect of each solvent in the target products adsorption capacity and selectivity for each of the tested solid

materials. On the basis of an extensive literature review, Amberlyst-15, Amberlyst-35, and H-BEA25 zeolite were used as catalysts in this work.

2.4. Reaction Kinetics Experiments. The experimental setup used in the batch reaction experiments is depicted in Figure 3. The reaction experiments took place in a glass-jacketed autoclave (1), model Buchiglaususter (Germany), with a maximum capacity of 1 dm³. The catalyst was placed in the basket (4), which has two positions: initially, it was located out of the liquid; when the experiment starts, it rolled down through the shaft and was immersed into the liquid. The start of the experiment and the immersion of the catalyst basket were triggered by turning on the stirrer (7). The mechanical stirrer has a maximum adjustable speed between 0 and 2200 rpm and is powered by a three-phase motor with 0.33 kW. The continuous circulation of oil through the jacket of the autoclave maintained the system at the predefined temperature. The silicon oil was heated in a thermostatic bath (11) Ecoline 006/E300 (Lauda, Germany). The temperature of the experiment was measured by a thermocouple (8), which was monitored by a computer. The autoclave, pressurized with helium during the experiment, is equipped with a manometer (10) and a pressure sensor, which are also monitored by a computer. The valves of the feed container (6) allow the depressurization of the system. The air-actuated sampling valve

(9) is controlled by a computer. The composition of all the samples collected during the reaction experiments was determined through the analytical method described in Section 2.2, and this information was used to determine the limiting reactant conversion (simply referred to as conversion in the remainder of this work).

To study the effect of mass transfer on the reaction kinetics, several experiments with different stirring speeds were carried out, in order to determine the minimum stirring speed capable of making the external mass-transfer effects become negligible. The reaction mixtures were composed by a 1:2 ratio of acetone and glycerol diluted in 30% of solvent (molar basis). Amberlyst-35 resin (0.5 wt % considering total reactant mass) was used as the catalyst. The experiments were carried out for 8 h at 600, 750, and 900 rpm.

Then, in order to determine reaction kinetics parameters, several experiments were defined, as described in Table 3.

Table 3. Reaction Experiments Operating Conditions

experiment ID	temperature (K)	A/G (n/n)	$x_{solvent}$ (n/n)	catalyst loading (%wt$_{cat}$/wt$_{Reactants}$)
Exp01	303	1.0	0.5	0.5
Exp02	313	1.0	0.5	0.5
Exp03	323	1.0	0.5	0.5
Exp04	303	2.0	0.5	0.5
Exp05	303	0.5	0.5	0.5
Exp06	313	2.0	0.5	0.5
Exp07	313	0.5	0.5	0.5
Exp08	303	1.0	0.7	0.5
Exp09	323	1.0	0.3	0.5
Exp10	323	1.0	0.7	0.5
Exp11[a]	323	1.0	0.5	0.25
Exp12[a]	323	1.0	0.5	0.25

[a]Average catalyst particle radius of 290 μm for Exp11 and 435 μm for Exp12 (for all the remaining experiments, the average catalyst particle radius was 390 μm).

3. THEORETICAL

3.1. Mathematical Modeling. In order to predict the dynamic behavior of the batch reactor and to determine the kinetic parameters of glycerol ketalization, in the presence of ethanol, a mathematical model was developed. The reactor was assumed to work under perfectly stirred conditions, and therefore, the composition of the liquid phase is the same at all positions of the reactor at a given instant. The model takes into account isothermal operation and assumes that the internal mass-transfer resistance is limited to macropore diffusion, following Fick's diffusion Law and considering that the catalyst is composed of spherical particles. Further details regarding the model can be found elsewhere.[53,54] Note that the operating conditions were set in order to ensure that the external mass-transfer limitations were negligible.

The bulk and particle mass balance equations to component i are presented by eqs 1 and 2, respectively,

$$\frac{\partial C_{b,i}}{\partial t} = -\left(\frac{1-\varepsilon_b}{\varepsilon_b}\right)\frac{3}{r_p}D_{eff,i}\frac{\partial C_{p,i}}{\partial r}\bigg|_{r=r_p} \tag{1}$$

$$\varepsilon_p\frac{\partial C_{p,i}}{\partial t} = \frac{1}{r^2}\frac{\partial}{\partial r}\left(D_{eff,i}r^2\frac{\partial C_{p,i}}{\partial r}\right) + (1-\varepsilon_p)v_i\rho_s\Re \tag{2}$$

where $C_{b,i}$ and $C_{p,i}$ represent the bulk concentration and the concentration in the particle pores of component i, respectively, ε_b and ε_p are the bulk porosity and particle porosity, respectively, $D_{eff,i}$ is the effective diffusion coefficient, r_p is the particle radius, v_i, ρ_s, and $\Re$ represent the stoichiometric coefficient of component i, solid density, and reaction rate along the catalyst particle radius, t is the time, and r is the radial position within the particle.

Initial and boundary conditions are given by eqs 3−6

$$t = 0 \quad C_{b,i} = C_{b,i0} \tag{3}$$

$$t = 0 \quad C_{p,i} = C_{p,i0} \tag{4}$$

$$r = 0 \quad \frac{\partial C_{p,i}}{\partial r} = 0 \tag{5}$$

$$r = r_p \quad C_{b,i} = C_{p,i}|_{r=r_p} \tag{6}$$

The infinite dilution diffusivities can be estimated by the Scheibel correlation (eq 7).[55]

$$D_{i,j}^0 = \frac{8.2\times10^{-8}T}{\eta_j V_{M,i}^{1/3}}\left[1 + \left(\frac{3V_{M,j}}{V_{M,i}}\right)^{2/3}\right] \tag{7}$$

$D_{i,j}^0$ is the diffusion coefficient for a dilute solute i in a solvent j, T is the temperature, η_j is the viscosity of solvent j, and V_M is the molar volume.

For multicomponent systems, the Perkins and Geankoplis correlation[56] can be used to predict the molecular diffusivity coefficient of a compound in a mixture, $D_{i,m}$ (eq 8)

$$D_{i,m}\eta_m^{0.8} = \sum_{\substack{j=1 \\ j\neq i}}^{n} x_j D_{i,j}^0\eta_j^{0.8} \tag{8}$$

where η_m is the viscosity of the mixture and η_j is the viscosity of the component j. The effective diffusion coefficients are then estimated by eq 9.

$$D_{eff,i} = \frac{\varepsilon_p D_{i,m}}{\tau} \tag{9}$$

The reaction rate for the ketalization of glycerol has been described by several models, such as Pseudo-Homogeneous (PH),[57] Eley−Rideal (ER),[46,58] and Langmuir−Hinshelwood−Hougen−Watson (LHHW) models.[49,53,57,59]

The simplest approach is the PH model that considers a reversible reaction of first order in each species and can be expressed also in terms of activities as

$$\Re = k_c\left(a_{Ac}a_{Gly} - \frac{a_{Solk}a_w}{K_{eq}}\right) \tag{10}$$

where k_c is the reaction kinetic constant, K_{eq} is the reaction thermodynamic equilibrium constant, and a_i is the activity coefficient of each species. To determine the activity coefficients, the universal functional activity coefficient (UNIFAC) model was used. This group contribution method uses the surface areas and relative molecular volumes of each species as parameters as well as the interaction parameters between the different groups of each molecule.

In the LHHW model, the most widely used for this kind of reaction, both reactants are adsorbed, followed by a surface

reaction that originates a hemiacetal. Two subsequent surface reactions lead to the formation of the adsorbed water and acetal. The final step consists of the desorption of both products. The rate-determining step is considered to be the surface reaction leading to the formation of adsorbed hemiacetal. Some literature suggests that water adsorption is significantly higher than that of the remaining species involved in the reaction; thus, neglecting the adsorption of those species is commonly accepted. Equation 11 presents the simplified reaction rate expression, in terms of activities, used to describe the experimental data, considering the previously mentioned assumptions

$$\Re = k_c \frac{a_{Ac} a_{Gly} - \frac{a_{Solk} a_w}{K_{eq}}}{(1 + K_{S,W} a_W)^2} \tag{11}$$

where $K_{S,W}$ is the adsorption equilibrium constant for water.

The ER model is similar to the LHHW model, but it is based on the assumption that only one of the molecules adsorbs onto the solid, while the other reacts with it directly from the fluid phase.

$$\Re = k_c \frac{a_{Ac} a_{Gly} - \frac{a_{Solk} a_w}{K_{eq}}}{1 + K_{S,W} a_W} \tag{12}$$

According to the centered form of the Arrhenius law, kinetic constant depends on temperature,

$$k_c = k_{c_0} \exp\left[-\frac{E_a}{R}\left(\frac{1}{T} - \frac{1}{T_{ref}}\right)\right] \tag{13}$$

In this equation, k_{c_0} represents the pre-exponential term, R represents the universal gas constant, and the reference temperature, T_{ref}, was 313 K.

The reaction thermodynamic equilibrium constant, K_{eq}, can be determined by the following equation

$$K_{eq} = \frac{a_{Solk} a_W}{a_{Ac} a_{Gly}} \tag{14}$$

The chemical equilibrium constant can be expressed as a function of the reaction standard Gibbs free energy, ΔG^0, and temperature, T, known as the Van't Hoff law

$$K_{eq} = e^{-\Delta G^0/RT} \tag{15}$$

Furthermore,

$$\Delta G^0 = \Delta H^0 - T\Delta S^0 \tag{16}$$

where ΔS^0 is the standard entropy and ΔH^0 is the standard enthalpy. Combining both equations, a linear correlation, ln K_{eq} vs $1/T$ (K^{-1}), is obtained

$$\ln K_{eq} = \frac{\Delta S^0}{R} - \frac{\Delta H^0}{R} \frac{1}{T} \tag{17}$$

3.2. Numerical Solution. The numerical solution of this problem was obtained using the commercial software General PROcess Modelling System (gPROMS) version 4.2.0, using a method of orthogonal collocation in finite elements; to this end, the radial dimension of the catalyst was discretized in 30 finite elements with two interior collocation points in each finite element, and the Differential-Algebraic equation solver (DASOLV) integrated in the software was used to solve the remaining system of ordinary differential equations in time.

gPROMS software was also used to estimate the values of the unknown parameters, namely, E_a and k_{c_0} for the PH model and E_a, k_{c_0}, and $K_{S,W}$ for the ER and LHHW models, by using the "Parameter Estimation" tool. The experimental data was fitted by the maximum likelihood method through the following objective function

$$\Phi = \frac{N}{2}\ln(2\pi) + \frac{1}{2}\min_\theta\left\{\sum_{j=1}^{NE}\sum_{k=1}^{NM_j}\left[\ln(\sigma_{jk}^2) + \frac{(X_{jk}^{exp} - X_{jk}^{mod})^2}{\sigma_{jk}^2}\right]\right\} \tag{18}$$

where N represents the total number of measurements during all the experiments, θ is the set of parameters to be estimated, σ_{jk}^2 is the variance in conversion, X_{jk}^{exp} and X_{jk}^{mod} are the kth measured and predicted values, respectively, for the conversion in experiment j. NE represents the number of experiments performed, and NM$_j$ is the number of measurements of conversion values obtained in experiment j. For all simulations, a tolerance of 10^{-5} was used.

4. RESULTS AND DISCUSSION

4.1. Ketalization Solvent and Catalyst Selection. The solvent selection methodology applied in the present work, which was specifically developed for identifying potential solvents for sorption-enhanced reactive processes,[49] comprises an initial stage in which approximately 100 of the most commonly used industrial solvents are ranked on the basis of their physical−chemical properties followed by a set of reaction and adsorption tests carried out with the top ranked solvents. During the theoretical screening stage, solvents that have been reported as reactive with any of the reactants or products of the studied ketalization reaction were eliminated from the primary list. The solvents remaining from the previous preselection step were ranked considering a weight of 50% for process performance and miscibility parameters (12.5% for dipole moment, 12.5% for dielectric constant, and 25% for the Hildebrand solubility parameter) and 50% for process impact parameters (25% for lethal dose, LD$_{50}$, and NFPA health hazard classification; 25% for octanol−water partition coefficient, log P$_{ow}$, and persistence time). For each variable, a score of 100% was attributed to the solvent that presented the higher value for that variable and a score of 0%, for the lower value, if the variable analyzed is intended to be maximized. All the other solvents were scored proportionally. The inverse scoring procedure was applied to variables that were intended to be minimized. The full solvents ranking and their properties can be found in the Supporting Information. At this point, it was decided to proceed to the second stage of the solvent selection methodology with only the three most promising solvents: methanol, dimethyl sulfoxide, and ethanol (which scored 70%, 70%, and 66%, respectively, according to the methodology applied). This allowed one to conduct the necessary reaction and adsorption tests for the solvent selection in parallel with the catalyst screening tests, keeping the overall number of experiments within reasonable limits. Amberlyst-15, Amberlyst-35, and H-BEA25 zeolite were selected as catalysts, given their potential for sorption-enhanced processes comprising ketalization reactions according to the data reported in the open literature.

The first goal of the reaction tests performed within the frame of the solvent selection methodology was to verify if the solvents would react with any of the species involved in the ketalization reaction. Moreover, to observe the influence of the
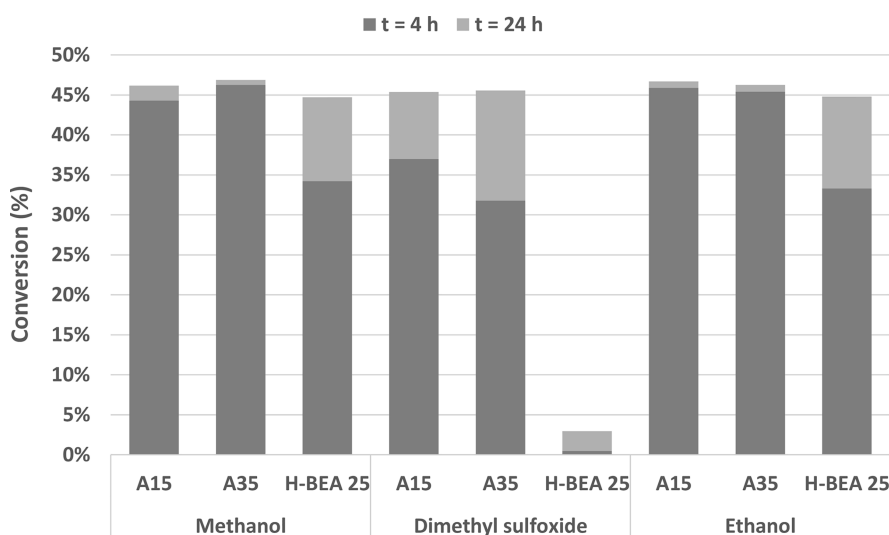
Figure 4. Comparison of the performance of the catalysts on the kinetics of the ketalization of glycerol after 4 and 24 h (T = 313 K; P = 1 bar; A/G = 1.0; x_{solv} = 0.5; cat. loading of 1.0 wt % of the total reactant mass).

presence of the catalysts in the kinetics of the reaction between glycerol and acetone, experimental tests were carried out using different catalysts. A comparison of the ketalization kinetics performance of the tested catalysts, Amberlyst-15, Amberlyst-35, and H-BEA 25, is depicted in Figure 4.

Catalysts Amberlyst-15 and Amberlyst-35 presented similar kinetic performances, achieving conversions above 40% after 4 h, independently of the solvent used. This was not the case when H-BEA25 was used as the catalyst. Lower conversion rates were observed for the zeolite than for the ion-exchange resins tested. Reaction kinetics does not seem to be affected by the use of ethanol or methanol as solvents. However, the use of dimethyl sulfoxide delays the reaction. It is possible that this solvent may cause mass-transfer issues or, alternatively, that it might adsorb strongly in the catalysts hindering the access to its active sites. Finally, it must be mentioned that no secondary product formation was observed during any of the experiments.

The main objective of the adsorption tests was to study the eluents interaction with the different adsorbents/catalysts in order to observe how this affects the adsorption capacity and selectivity of the ketalization reaction products (solketal and water). Through the outlet concentration histories obtained for water and solketal injections in fixed bed columns packed with Amberlyst-15, Amberlyst-35, and H-BEA using methanol, dimethyl sulfoxide, and ethanol as eluents, it was possible to determine the mean residence time of those species within the bed (Table 4).

Table 4. Average Retention Times of Pulses of Solketal and Water in Fixed Bed Columns Packed with Amberlyst-15, Amberlyst-35, and H-BEA 25 Using Methanol, Dimethyl Sulfoxide, and Ethanol as Eluent at 313 K

solvent	Amberlyst-15		Amberlyst-35		H-BEA 25	
	solketal	water	solketal	water	solketal	water
methanol	3.0	8.8	3.3	10.8	2.0	4.8
dimethyl sulfoxide	3.5	5.8	3.0	4.8	3.5	4.8
ethanol	3.0	8.8	3.8	11.8	2.5	3.8

The results obtained allowed one to conclude that, when dimethyl sulfoxide is used as eluent, the retention time for water is significantly reduced, when compared with the other eluents, which likely is a consequence of strongly competitive adsorption between water and dimethyl sulfoxide. This, together with the lowest catalytic performance in the presence of dimethyl sulfoxide, leads to the exclusion of this species as a potential solvent for further studies. From Table 4, it is also possible to verify that H-BEA 25 has a relatively low selectivity toward water adsorption over solketal, since the absolute retention times and the difference between the retention times of those two species are smaller than for the ion-exchange resins tested. On the other hand, Amberlyst-15 and Amberlyst-35 resins have similar performances when using ethanol and methanol as eluents. However, when ethanol and Amberlyst-35 are used simultaneously as the mobile and stationary phase, the largest difference between solketal and water retention times was registered, meaning that the selectivity toward the target products can be considerably enhanced with this combination of liquid and solid phases. This is a key parameter for the selection of the most suitable solvent since a sorption-enhanced reactive process can take advantage of such differences in the adsorption properties, extending the limiting reactant conversion beyond the values imposed by the thermodynamic equilibrium through the implementation of the adequate dynamic operating mode, as reported elsewhere for similar reactive systems.[60] Moreover, the absolute retention times are higher than those reported in the other experiments, suggesting that ethanol will be less adsorbed in the catalyst active sites. Given the aforementioned information, the solvent selection methodology applied and the experimental tests performed with different materials allowed one to identify ethanol and Amberlyst-35 as the most suitable solvent and catalyst for the synthesis of solketal.

4.2. Reaction Thermodynamic Parameters Estimation. All the experiments described in Table 3 and Section 2.4 were carried out until no changes were observed in the bulk composition for at least 2 h. The thermodynamic equilibrium was assumed to be reached under these conditions. The experimental values of the equilibrium constant were determined through eq 14, taking into account the final

composition of the reactor operated under isothermal conditions and computing the respective activities. Figure 5
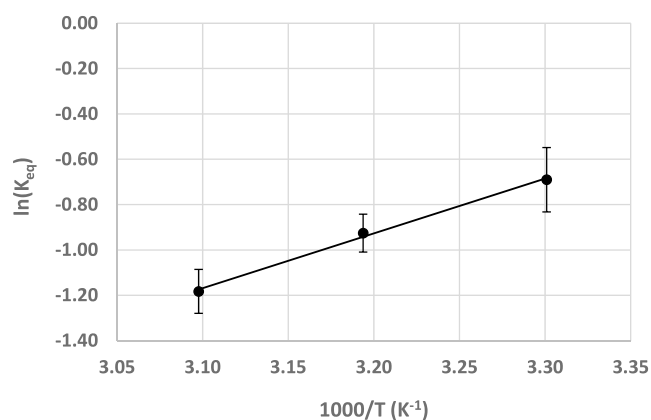

Figure 5. Linearization of K_{eq} versus $1/T$ for all experiments performed (operating conditions: 750 rpm, 8 bar, $m_{catalyst}$ = 0.5 wt % reactants).

presents the linearization of the dependence of the equilibrium constant with temperature (eq 17) that allows the determination of the standard entropy, ΔS^0, and the standard enthalpy, ΔH^0.

According to these results, the dependence of the equilibrium constant on temperature can be expressed as ln K_{eq} = −8.665 + 2418/T. The standard enthalpy and Gibbs free energy could then be predicted, and the estimated values were −20.1 ± 1.1 kJ ± mol^{-1} and 1.4 ± 0.1 kJ ± mol^{-1}, respectively.

The results confirmed the exothermal character of the studied reaction since the estimated enthalpy value was negative, which implies that the equilibrium conversion decreases as temperature increases. Several authors withdrew the same conclusion for several ketalization and acetalization reactions involving glycerol and short-chained ketones and aldehydes.[34,44,57]

Nanda et al.[44] published a study of the ketalization of glycerol with acetone for the production of solketal in which ethanol was also used as solvent, and the most relevant thermodynamic equilibrium parameters were determined: ΔH^0 = −30.1 ± 1.6 kJ ± mol^{-1}; ΔG^0 = −2.1 ± 0.1 kJ ± mol^{-1}. The values are slightly different from those obtained in this work; however, the previous authors neglected the nonideal behavior of the reaction media, and all the reaction thermodynamic parameters were estimated on the basis of molar concentration values. This fact emphasizes the relevance of including this aspect in the determination of such thermodynamic properties.

4.3. Reaction Kinetics Studies. A detailed study of the kinetic behavior of the reaction between acetone and glycerol catalyzed by Amberlyst-35 and using ethanol as solvent was conducted. The effect of several variables in the reaction rate was evaluated in order to determine the most suitable reaction rate law for the description of the performed batch reactor

experiments and to determine the corresponding kinetic parameters.

For this purpose, preliminary tests to assess the extent of mass-transfer resistances were performed. External mass transfer can play a major role by limiting the overall reaction rate in heterogeneously catalyzed systems. In the system studied in this work, this effect can be even higher considering that acetone and glycerol have limited miscibility in the absence of the reaction products, which underlines the importance of using a solvent in the reaction media. The performance of the reaction was evaluated at different stirring speeds from 600 to 900 rpm.

From the experiments carried out, it was possible to say that, after 200 min, the reaction reached the equilibrium. A maximum conversion of 70% was obtained. Through the experiments performed at a stirring speed of 900 and 750 rpm, it was possible to observe that the conversion history had the same evolution, meaning that the reaction rate was not affected by the external mass transfer and the limitations associated with this phenomena could be suppressed if the stirring speed is set to 750 rpm. Given the aforementioned information, subsequent experiments were carried out at 750 rpm.

The impact of internal mass-transfer resistances was also assessed by performing experiments using catalyst with different particle size distributions. The experiments were carried out at the highest temperature tested in this work (323 K) since mass-transfer effects become more significant than kinetic effects under such conditions. The experiments performed with an average catalyst diameter of 580 μm (sieved catalyst) lead to a faster conversion of the limiting reactant compared with the experiments performed with catalyst particles with a diameter of 780 μm (unsieved catalyst). These results indicate that internal mass transfer has a considerable contribution to the kinetic behavior of this reactive system and cannot be neglected. This topic will be discussed in further detail in Section 4.3.2, and the findings agreed with the simulation results.

4.3.1. Reaction Kinetic Parameters Estimation. As previously stated, the estimation of the kinetic parameters was performed by fitting the results obtained with the mathematical model described in Section 3.1 to the experimental results obtained for the experiments performed in a batch reactor under the conditions reported in Table 3. The parametric study carried out allowed one to determine the unknown parameters of each of the three reaction rate laws considered for this system, namely, PH, LHHW, and ER.

In a first stage, the initial reaction rate method was applied for the determination of a first estimate of the activation energy considering the observed reaction rate (excluding the experiment performed with a different particle size distribution) and assuming the Arrhenius Law for the dependence of the reaction rate constant with temperature. A value of 36.1 ± 6.3 kJ ± mol^{-1} was estimated for the activation energy, which was used as the initial guess in the parameter estimation performed subsequently.

Table 5. Estimated Kinetic Parameters for the Different Models and Goodness of Fit Values

model	E_a (kJ mol^{-1})	k_{c_0} (mol kg$_{cat}^{-1}$ s^{-1})	$K_{S,W}$	R^2	F_{obj}
PH	63.8 ± 10.1	177 ± 18		0.942	−447
LHHW	69.0 ± 6.6	492 ± 93	14.4 ± 3.1	0.961	−475
ER	67.4 ± 6.6	528 ± 153	47.7 ± 20.0	0.956	−473

The quality of the fitting was evaluated taking into account the value of the objective function used in the estimation (eq 18), a goodness-of-fit analysis based on the 95% chi-squared criterion, and a correlation coefficient computed through eq 19.

$$R^2 = 1 - \frac{\sum_{j=1}^{NE} \sum_{k=1}^{N} (X_{jk}^{exp} - X_{jk}^{mod})^2}{\sum_{j=1}^{NE} \sum_{k=1}^{N} (X_{jk}^{exp} - \bar{X}^{exp})^2} \tag{19}$$

The results of the parameter estimation for the studied reaction rate laws are presented in Table 5.

It is worth mentioning that the chi-squared goodness-of-fit test at 95% verified that there was a statistically accurate representation of the experimental data by the implemented mathematical model regardless of the reaction rate law used. Nevertheless, from the results presented in Table 5, it can be observed that the lowest objective function and the highest correlation coefficient values were attained when describing the reaction rate law by the LHHW model, suggesting that this is the most accurate description of the reaction mechanism among the tested models. In fact, the correlation coefficient value determined, 0.961, indicates that the model was able to predict the experimental kinetic data for this reaction with high accuracy over the wide range of conditions tested. Moreover, the errors associated with the parameters estimated for the LHHW model are also lower than those determined for the remainder models.

The estimated activation energy value assuming a LHHW reaction rate law was 69.0 ± 6.6 kJ $\pm$ mol^{-1}, which is almost double the value obtained with the initial reaction rate method previously reported. This fact supports the existence of considerable mass-transfer limitations, as stated earlier, and the same trend could be observed, independently of the reaction rate law proposed. The activation energy value estimated in this work is within the range of the values reported in the open literature for similar systems. For instance, Nanda et al.[44] reported an activation energy of 55.6 ± 3.1 kJ $\pm$ mol^{-1} for this system; however, in that study, the nonideal behavior of the mixture was not accounted for since all the estimations were performed on the basis of the reactor composition in terms of molar amounts and, more importantly, the impact of the internal mass transfer was neglected without any experimental evidence, contrasting to what was demonstrated in the present study. Esteban et al.[46] used another ion-exchange resin as catalyst for this reaction, Lewatit GF101, in the absence of solvent. A value of 124.0 ± 12.9 kJ $\pm$ mol^{-1} was found for the activation energy assuming the ER mechanism as the best hypothesis among the large number of reaction rate laws tested. The reactions of glycerol with formaldehyde,[61] acetaldehyde,[62] or butyraldehyde[63] catalyzed by Amberlyst-47 have also been previously studied with the respective authors reporting activation energy values ranging between 55 and 60 kJ $\pm$ mol^{-1}, assuming a PH reaction rate law.

It is important to mention that the dependence of the adsorption equilibrium constant with temperature, typically described by the Van't Hoff law, was also considered in the present work. Those results are not presented since the introduction of the pre-exponential factor and the adsorption enthalpy lead to an excessive increase in the errors associated with all the estimated parameters as a consequence of the increase of the number of parameters to be estimated. Nevertheless, as the difference between the maximum and minimum operating temperatures does not exceed 20 K, the effect of temperature in this variable was considered negligible, as proposed in previous works.[49]

A detailed analysis regarding the effect of the most relevant reaction variables on the reaction kinetics and regarding the ability of the mathematical model and reaction rate law proposed to describe the results obtained during the parametric study performed is provided in the following section.

4.3.2. Effect of Temperature, Initial Reactants Ratio, Solvent Ratio, and Internal Mass Transfer on the Reaction Rate.

In the present work, the reaction between glycerol and acetone was carried out under isothermal conditions with temperatures ranging from 303 to 323 K to evaluate the impact of this variable on the reaction rate. Figure 6 shows the
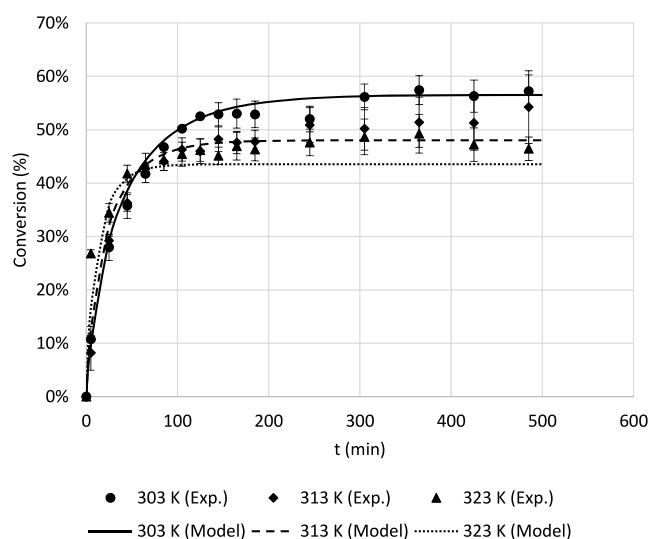
Figure 6. Effect of temperature on the reaction rate (P = 8.0 bar, A/G = 1.0, x_{solv} (n/n) = 0.50, catalyst load = 0.5 wt % of the total mass of reactants, stirring speed = 750 rpm).

experimental data regarding the evolution of the conversion with time at 303, 313, and 323 K, using equimolar amounts of the reactants diluted in 50% (n/n) of ethanol as well as the mathematical model prediction assuming the LHHW rate law with the parameters previously estimated.

As expected, Figure 6 demonstrates that, as temperature increases, the reaction rate becomes higher. On the other hand, the equilibrium conversion value decreases since this is an exothermic reaction as previously stated. It is also possible to observe that the model implemented and the estimated parameters were able to accurately describe this behavior, in terms of both the reaction kinetics and the reaction thermodynamic equilibrium.

The initial reaction media composition strongly affects the rate of conversion of the limiting reactant. This variable is particularly important in systems comprising nonideal mixtures as in this case. In Figure 7, the effect of the initial reactants molar ratio on the conversion over time is presented. Nevertheless, the studied initial reactants molar ratio values were kept around unity (more precisely between 0.5 and 2.0) since such values are usually preferred to maximize the produced amount of the target product and do not negatively affect the overall process productivity or complicate downstream separation processes as using reactants in excess
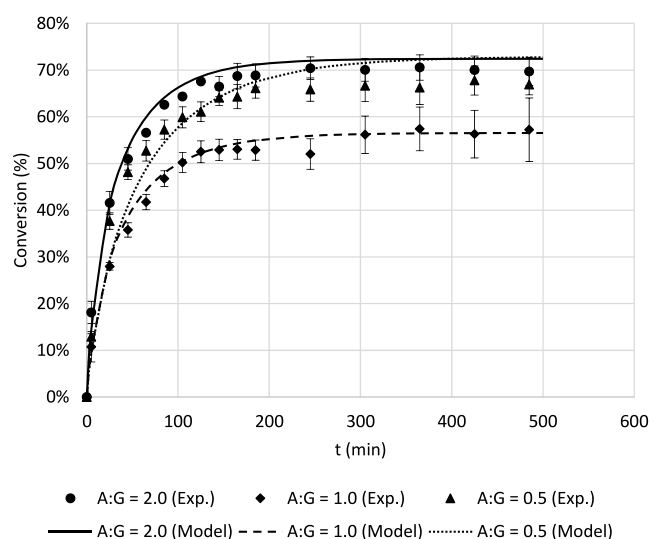
Figure 7. Effect of the initial reactants molar ratio on the reaction rate ($P = 8.0$ bar, $T = 303$ K, x_{solv} (n/n) = 0.50, catalyst load = 0.5 wt % of the total mass of reactants, stirring speed = 750 rpm).

Figure 8. Effect of the solvent molar fraction on the reaction rate ($P = 8.0$ bar, $T = 303$ K, A/G = 1.0, catalyst load = 0.5 wt % of the total mass of reactants, stirring speed = 750 rpm).

typically does. These issues are even more relevant for integrated reactive-adsorption processes.

The reactive media composition affects, simultaneously, the reaction rate, the equilibrium conversion, and the mass transfer within the catalyst particles. The experimental results from Figure 7 show that, as it is widely accepted, the use of an excess of one of the reactants increases both the reaction rate and the equilibrium conversion when compared to the use of the stoichiometric amount of the reactants. These results also demonstrate that the highest limiting reactant conversion rate was achieved for an acetone/glycerol molar ratio of 2. The differences observed in the reaction rate when using either acetone or glycerol in excess are related with the respective increase or decrease of the diffusion coefficients inside the catalyst pores under those specific conditions. As the studied reactive system presents considerable internal mass-transfer resistances, the use of acetone, which has more favorable transport properties than glycerol (lower viscosity and lower density, for instance), reduces the impact of this phenomena in the observed reaction rate. Figure 7 also shows a good agreement between the experimental data and the mathematical model predictions, which highlights the importance of including the internal mass-transfer resistances and the nonideality of the mixture in the model for a more accurate description of the overall process.

The effect of the amount of ethanol added to the reactive mixture in the kinetics was also studied, as it can be seen in Figure 8. The studied solvent concentration range was defined, not only taking into account the partial miscibility of the reactants but also considering the high dilution factor typically imposed by the significantly large amounts of eluent used for regeneration purposes in sorption-enhanced reactive processes (particularly for the desorption of water from strong acid ion-exchange resins).

It was possible to observe that the initial ethanol concentration has a minor impact on the evolution of the solketal yield over time within the concentration range studied. Nevertheless, the mathematical model was able to account for those small differences as well. The lower reaction rate observed for the experiment performed with a higher amount
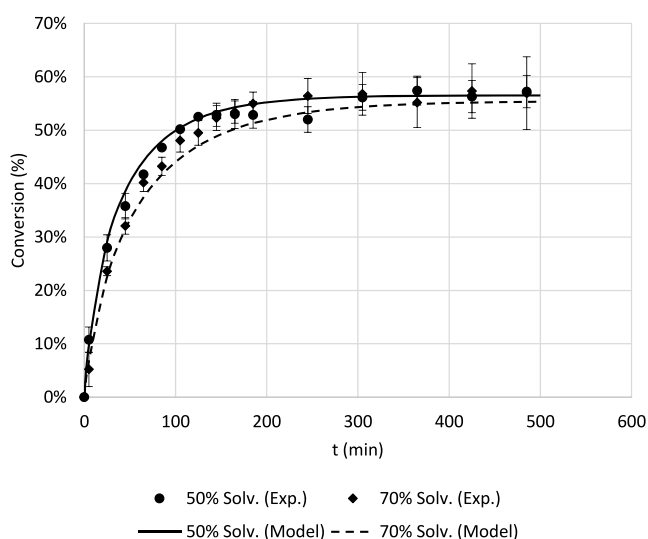
of solvent can be explained by the lower concentration of the reactive species, which according to the collision theory decreases the interaction between the reactants molecules, resulting in a reduction of the reactant conversion rate. In the present work, all the experiments were performed in the presence of a solvent, and therefore, no direct comparison could be made with the conversions attained under solvent-free conditions. Moreover, the data reported by different research groups for the studied ketalization reaction in the absence of solvents presents some consistency issues, and it is difficult to find experimental results attained in the same conditions as those studied in this work since, when working under solvent-free conditions, higher amounts of acetone and higher temperatures are typically employed to minimize the miscibility problems and accelerate the reaction rate. For instance, in the work reported by Manjunathan et al.,[39] glycerol conversion values above 80% were attained at equilibrium conditions using zeolite beta as catalyst and an initial acetone to glycerol molar ratio of 2.0 without the presence of a solvent at approximately 303 K. This value is significantly larger than that determined in this work in the presence of ethanol. On the other hand, the research reported by Esteban et al.,[46] using Lewatit GF101 resin as the catalyst under solvent-free conditions, indicates that the solketal yield at equilibrium conditions at 313 K for a reaction mixture initially containing acetone and glycerol in a 3 to 1 molar ratio would be only slightly higher than 30%; however, the glycerol conversion value determined in this work for the same temperature and for equimolar amounts of the reactants was approximately 50%. Despite the different methodologies applied (different sample treatments prior to analysis, the use of the different performance parameters, as reactant conversion values or product yields, among others), the examples previously provided clearly demonstrate the consistency issues previously mentioned for the solvent-free ketalization reaction data. On the other hand, the results obtained in this work for a 2.0 acetone to glycerol ratio at 303 K were similar to those report by Nanda et al.,[44] for these particular conditions, despite the use of different amounts of ethanol as solvent. Nevertheless, the effect of the introduction of a solvent in the reaction media

shall not be limited to the rate at which the reactants are converted as demonstrated in Figure 8. This issue has already been addressed in Section 4.1 in which it was demonstrated that the use of dimethyl sulfoxide negatively affected the maximum reactants conversion. Oliveira et al.[64] also demonstrated that a higher glycerol conversion could be obtained when using dimethyl formamide as solvent than when using dimethyl sulfoxide under the same operating conditions (323 K and a 2.0 acetone to glycerol molar ratio). Hence, the use of solvents can simultaneously change the reaction kinetics and thermodynamic equilibrium since it affects the reactant and product concentrations, it modifies the interaction between species (accounted for in this work by the introduction of activity coefficients in the model), and it can change the species reactivity by solvation.

Although the existence of considerable internal mass-transfer limitations has already been addressed throughout this work, two batch reaction experiments were performed at the highest temperature within the studied range using catalyst particles presenting different size distributions (Figure 9).
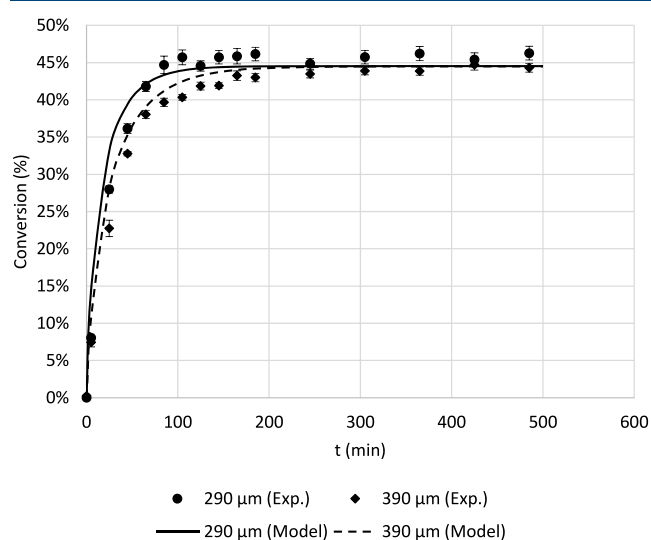

Figure 9. Effect of the catalyst particle radius on the reaction rate ($P =$ 8.0 bar, $T = 323$ K, A/G = 1.0, x_{solv} (n/n) = 0.50, catalyst load = 0.25 wt % of the total mass of reactants, stirring speed = 750 rpm).

As demonstrated in Figure 9, the reactants were converted at higher rates when catalyst particles with a radius of 290 μm (sieved resin) were used, compared to the experiment performed with an average catalyst particle radius of 390 μm (unsieved resin). This fact is strictly related to the decrease of the contribution of internal mass transfer to the overall reaction rate for smaller particles. To quantify the effect of the diffusion mechanism on the observed reaction rate, the effectiveness factor, η, was computed as a function of the particle radius.[54] Considering the average unsieved particle diameter, an effectiveness factor lower than 0.1 was determined ($T = 303$ K, A/G = 1.0, x_{solv} (n/n) = 0.50), supporting the conclusion that the reaction occurs under diffusion controlled conditions. To be operating in a completely chemically controlled regime, the effectiveness factor must be approximately 1. For this material, at 303 K, an average catalyst particle diameter of less than 10 μm would be required. Such fine particles are not commercially available and cannot be obtained from the commercial resin.

5. CONCLUSIONS

The work presented reports a detailed study of the glycerol ketalization reaction, for the synthesis of solketal, from the selection of the most suitable catalyst and solvent for this reaction to the description of its thermodynamic equilibrium and kinetics.

The screening of commercial catalysts showed that acid ion-exchange resins have higher activities than zeolite H-BEA25. From the catalysts tested, one can conclude that the best kinetic performance was obtained when using Amberlyst-35. On the other hand, the solvent selection methodology applied in this work, which was specifically developed for integrated reactive–adsorptive processes, identified ethanol as the most suitable solvent for this system.

Chemical equilibrium data was gathered for temperatures ranging from 303 to 323 K. The standard enthalpy and Gibbs free energies were found to be -20.1 ± 1.1 kJ mol^{-1} and 1.4 ± 0.3 kJ mol^{-1}, respectively, using the UNIFAC method to determine the activities of each species. From the batch reactor experiments, all the results were obtained after ensuring that the experiments were performed in the absence of external mass-transfer limitations. The experimental results revealed that the reaction kinetics behavior could be accurately described by the LHHW reaction rate law, considering the presence of internal mass-transfer resistances. The model considers the surface reaction between the adsorbed reactants that leads to the formation of water as the rate determining step. The activation energy value estimated for the reaction was 69.0 ± 6.6 kJ mol^{-1}, which is within the range of values reported in the open literature for similar reactive systems. The experimental results also demonstrate that, as expected for highly polar ion-exchange resins in the H$^+$-form, water adsorption must be taken into account for the description of the reaction kinetics for which a value of 14.4 ± 3.1 was estimated for the adsorption equilibrium constant.

■ ASSOCIATED CONTENT

S **Supporting Information**

The Supporting Information is available free of charge on the ACS Publications website at DOI: 10.1021/acs.iecr.9b03725.

Complete solvent selection methodology ranking (after the preselection stage) (PDF)

■ AUTHOR INFORMATION

Corresponding Author

*E-mail: ruifaria@fe.up.pt. Tel. +351 22 508 1578.

ORCID ⊙

Rui P. V. Faria: 0000-0002-1216-0613

Ana M. Ribeiro: 0000-0003-4269-1420

Alírio E. Rodrigues: 0000-0002-0715-4761

Notes

The authors declare no competing financial interest.

■ ACKNOWLEDGMENTS

NOMENCLATURE

Abbreviations

ER	Eley–Rideal model
LHHW	Langmuir–Hinshelwood–Hougen–Watson model
gPROMS	General Process Modelling System
PH	Pseudo-Homogeneous model
UNIFAC	Universal Functional Activity Coefficient

Variables

a_i	activity coefficient of component i
$C_{b,i}$	bulk concentration of component i, mol L^{-1}
$C_{p,i}$	average concentration in the particle pores of component i, mol L^{-1}
$C_{i,o}$	initial concentration in the liquid phase of component i, mol L^{-1}
$D_{i,j}^0$	diffusion coefficient for a dilute solute i in a solvent j, cm^2 s^{-1}
$D_{i,m}$	diffusion coefficient of compound i in a mixture, cm^2 s^{-1}
$D_{eff,i}$	effective diffusion coefficient, cm^2 s^{-1}
d_p	particle diameter, cm
D_m	molecular diffusivity, cm^2 s^{-1}
E_a	reaction activation energy, J mol^{-1}
k_{c_o}	Arrhenius equation pre-exponential term, mol kg^{-1} s^{-1}
k_c	reaction kinetic constant, mol kg^{-1} s^{-1}
K_{eq}	reaction thermodynamic equilibrium constant
$K_{S,W}$	adsorption equilibrium constants for water
$K_{S,EtOH}$	adsorption equilibrium constants for ethanol
N	total number of measurements during all experiments
NE	number of kinetic experiments performed
NM_j	number of measurements of conversion values taken in kinetic experiment j
P	pressure, bar
r	particle radial coordinate, cm
R	universal gas constant, J K^{-1} mol^{-1}
$\Re$	reaction rate, mol kg^{-1} s^{-1}
r_p	particle radius, cm
$V_{M,i}$	molar volume of component i, L mol^{-1}
T	temperature, K
T_{ref}	reference temperature, K
t	time, s
x_j	molar fraction of compound j
X_{jk}^{exp}	k^{th} value for the conversion measured in experiment j
X_{jk}^{mod}	k^{th} value for the conversion in experiment j predicted by the model
wt %	total weight percentage

Greek Letters

ε_b	bed porosity
ε_p	particle porosity
ΔG^0	reaction Gibbs free energy, J mol^{-1}
ΔH^0	standard enthalpy at 298 K, J mol^{-1}
ΔS^0	standard entropy at 298 K, J K^{-1} mol^{-1}
θ	set of parameters to be estimated by the maximum likelihood method
ν	stoichiometric coefficient
ρ_s	solid density, kg L^{-1}
η	liquid viscosity, g cm^{-1} s^{-1}
σ	variance
Φ	maximum likelihood objective function

REFERENCES

(1) Atabani, A. E.; Silitonga, A. S.; Badruddin, I. A.; Mahlia, T.; Masjuki, H.; Mekhilef, S. A comprehensive review on biodiesel as an alternative energy resource and its characteristics. *Renewable Sustainable Energy Rev.* **2012**, *16* (4), 2070–2093.

(2) Goodrum, J. W.; Geller, D. P.; Adams, T. T. Rheological characterization of animal fats and their mixtures with #2 fuel oil. *Biomass Bioenergy* **2003**, *24* (3), 249–256.

(3) Saraf, S.; Thomas, B. Influence of Feedstock and Process Chemistry on Biodiesel Quality. *Process Saf. Environ. Prot.* **2007**, *85* (5), 360–364.

(4) Leung, D. Y. C.; Wu, X.; Leung, M. K. H. A review on biodiesel production using catalyzed transesterification. *Appl. Energy* **2010**, *87* (4), 1083–1095.

(5) Ma, F.; Hanna, M. A. Biodiesel production: a review. *Bioresour. Technol.* **1999**, *70* (1), 1–15.

(6) Haas, M. J.; McAloon, A. J.; Yee, W. C.; Foglia, T. A. A process model to estimate biodiesel production costs. *Bioresour. Technol.* **2006**, *97* (4), 671–678.

(7) Oleoline Glycerine Market Report. http://www.hbi.fr/datas/media/590204fd077a6e381ef1a252/sample-quarterly-glycerine.pdf (accessed September 2017).

(8) Quispe, C. A. G.; Coronado, C. J. R.; Carvalho, J. A., Jr Glycerol: Production, consumption, prices, characterization and new trends in combustion. *Renewable Sustainable Energy Rev.* **2013**, *27* (0), 475–493.

(9) Ito, T.; Nakashimada, Y.; Senba, K.; Matsui, T.; Nishio, N. Hydrogen and ethanol production from glycerol-containing wastes discharged after biodiesel manufacturing process. *J. Biosci. Bioeng.* **2005**, *100* (3), 260–265.

(10) Byrd, A. J.; Pant, K. K.; Gupta, R. B. Hydrogen production from glycerol by reforming in supercritical water over Ru/Al2O3 catalyst. *Fuel* **2008**, *87* (13), 2956–2960.

(11) Slinn, M.; Kendall, K.; Mallon, C.; Andrews, J. Steam reforming of biodiesel by-product to make renewable hydrogen. *Bioresour. Technol.* **2008**, *99* (13), 5851–5858.

(12) Wen, G.; Xu, Y.; Ma, H.; Xu, Z.; Tian, Z. Production of hydrogen by aqueous-phase reforming of glycerol. *Int. J. Hydrogen Energy* **2008**, *33* (22), 6657–6666.

(13) Zhang, B.; Tang, X.; Li, Y.; Xu, Y.; Shen, W. Hydrogen production from steam reforming of ethanol and glycerol over ceria-supported metal catalysts. *Int. J. Hydrogen Energy* **2007**, *32* (13), 2367–2373.

(14) Menezes, A. O.; Rodrigues, M. T.; Zimmaro, A.; Borges, L. E. P.; Fraga, M. A. Production of renewable hydrogen from aqueous-phase reforming of glycerol over Pt catalysts supported on different oxides. *Renewable Energy* **2011**, *36* (2), 595–599.

(15) Wang, C.; Dou, B.; Chen, H.; Song, Y.; Xu, Y.; Du, X.; Zhang, L.; Luo, T.; Tan, C. Renewable hydrogen production from steam reforming of glycerol by Ni–Cu–Al, Ni–Cu–Mg, Ni–Mg catalysts. *Int. J. Hydrogen Energy* **2013**, *38* (9), 3562–3571.

(16) Schwengber, C. A.; Alves, H. J.; Schaffner, R. A.; da Silva, F. A.; Sequinel, R.; Bach, V. R.; Ferracin, R. J. Overview of glycerol reforming for hydrogen production. *Renewable Sustainable Energy Rev.* **2016**, *58*, 259–266.

(17) Sad, M. E.; Duarte, H. A.; Vignatti, C.; Padró, C. L.; Apesteguía, C. R. Steam reforming of glycerol: Hydrogen production optimization. *Int. J. Hydrogen Energy* **2015**, *40* (18), 6097–6106.

(18) Haider, M. H.; Dummer, N. F.; Knight, D. W.; Jenkins, R. L.; Howard, M.; Moulijn, J.; Taylor, S. H.; Hutchings, G. J. Efficient green methanol synthesis from glycerol. *Nat. Chem.* **2015**, *7* (12), 1028–1032.

(19) Carr, A. G.; Shi, X.; Domene, C.; Leung, A. K.; Green, W. H. Methanol formation from the treatment of glycerol in supercritical water and with ethylsulfide. *J. Supercrit. Fluids* **2016**, *117*, 80–88.

(20) Goetsch, D.; Machay, I. S.; White, L. R. *Production of methanol from the crude glycerol by-product of producing biodiesel.* US Patent US7388034B1, 2008.

(21) Gutiérrez Ortiz, F. J.; Serrera, A.; Galera, S.; Ollero, P. Methanol synthesis from syngas obtained by supercritical water reforming of glycerol. *Fuel* **2013**, *105*, 739−751.

(22) Posada, J. A.; Cardona, C. A. Design and analysis of fuel ethanol production from raw glycerol. *Energy* **2010**, *35* (12), 5286−5293.

(23) Oh, B.-R.; Seo, J.-W.; Heo, S.-Y.; Hong, W.-K.; Luo, L. H.; Joe, M.-h.; Park, D.-H.; Kim, C. H. Efficient production of ethanol from crude glycerol by a Klebsiella pneumoniae mutant strain. *Bioresour. Technol.* **2011**, *102* (4), 3918−3922.

(24) Lee, S. J.; Lee, J. H.; Yang, X.; Yoo, H. Y.; Han, S. O.; Park, C.; Kim, S. W. Re-utilization of waste glycerol for continuous production of bioethanol by immobilized Enterobacter aerogenes. *J. Cleaner Prod.* **2017**, *161*, 757−764.

(25) Stepanov, N.; Efremenko, E. Immobilised cells of Pachysolentannophilus yeast for ethanol production from crude glycerol. *New Biotechnol.* **2017**, *34*, 54−58.

(26) Trifoi, A. R.; Agachi, P. Ş.; Pap, T. Glycerol acetals and ketals as possible diesel additives. A review of their synthesis protocols. *Renewable Sustainable Energy Rev.* **2016**, *62*, 804−814.

(27) Serafim, H.; Fonseca, I. M.; Ramos, A. M.; Vital, J.; Castanheiro, J. E. Valorization of glycerol into fuel additives over zeolites as catalysts. *Chem. Eng. J.* **2011**, *178* (0), 291−296.

(28) Gadamsetti, S.; Rajan, N. P.; Rao, G. S.; Chary, K. V. R. Acetalization of glycerol with acetone to bio fuel additives over supported molybdenum phosphate catalysts. *J. Mol. Catal. A: Chem.* **2015**, *410*, 49−57.

(29) Nanda, M. R.; Yuan, Z.; Qin, W.; Ghaziaskar, H. S.; Poirier, M.-A.; Xu, C. Catalytic conversion of glycerol to oxygenated fuel additive in a continuous flow reactor: Process optimization. *Fuel* **2014**, *128* (0), 113−119.

(30) Cornejo, A.; Barrio, I.; Campoy, M.; Lázaro, J.; Navarrete, B. Oxygenated fuel additives from glycerol valorization. Main production pathways and effects on fuel properties and engine performance: A critical review. *Renewable Sustainable Energy Rev.* **2017**, *79*, 1400−1413.

(31) Samoilov, V. O.; Ramazanov, D. N.; Nekhaev, A. I.; Maximov, A. L.; Bagdasarov, L. N. Heterogeneous catalytic conversion of glycerol to oxygenated fuel additives. *Fuel* **2016**, *172*, 310−319.

(32) Okoye, P. U.; Abdullah, A. Z.; Hameed, B. H. Synthesis of oxygenated fuel additives via glycerol esterification with acetic acid over bio-derived carbon catalyst. *Fuel* **2017**, *209*, 538−544.

(33) Veluturla, S.; Narula, A.; D, S. R.; Shetty, S. P. Kinetic study of synthesis of bio-fuel additives from glycerol using a hetropolyacid. *Resource-Efficient Technologies* **2017**, *3*, 337.

(34) Nanda, M. R.; Zhang, Y.; Yuan, Z.; Qin, W.; Ghaziaskar, H. S.; Xu, C. Catalytic conversion of glycerol for sustainable production of solketal as a fuel additive: A review. *Renewable Sustainable Energy Rev.* **2016**, *56*, 1022−1031.

(35) Bozkurt, Ö. D.; Tunç, F. M.; Bağlar, N.; Çelebi, S.; Günbaş, İ. D.; Uzun, A. Alternative fuel additives from glycerol by etherification with isobutene: Structure−performance relationships in solid catalysts. *Fuel Process. Technol.* **2015**, *138*, 780−804.

(36) Mota, C. J. A.; da Silva, C. X. A.; Rosenbach, N.; Costa, J.; da Silva, F. Glycerin Derivatives as Fuel Additives: The Addition of Glycerol/Acetone Ketal (Solketal) in Gasolines. *Energy Fuels* **2010**, *24* (4), 2733−2736.

(37) Vicente, G.; Melero, J. A.; Morales, G.; Paniagua, M.; Martín, E. Acetalisation of bio-glycerol with acetone to produce solketal over sulfonic mesostructured silicas. *Green Chem.* **2010**, *12* (5), 899−907.

(38) Vol'eva, V. B.; Belostotskaya, I. S.; Malkova, A. V.; Komissarova, N. L.; Kurkovskaya, L. N.; Usachev, S. V.; Makarov, G. G. New approach to the synthesis of 1,3-dioxolanes. *Russ. J. Org. Chem.* **2012**, *48* (5), 638−641.

(39) Manjunathan, P.; Maradur, S. P.; Halgeri, A. B.; Shanbhag, G. V. Room temperature synthesis of solketal from acetalization of glycerol with acetone: Effect of crystallite size and the role of acidity of beta zeolite. *J. Mol. Catal. A: Chem.* **2015**, *396* (0), 47−54.

(40) Kowalska-Kus, J.; Held, A.; Nowinska, K. Enhancement of the catalytic activity of H-ZSM-5 zeolites for glycerol acetalization by

mechanical grinding. *React. Kinet., Mech. Catal.* **2016**, *117* (1), 341−352.

(41) Maksimov, A. L.; Nekhaev, A. I.; Ramazanov, D. N.; Arinicheva, Y. A.; Dzyubenko, A. A.; Khadzhiev, S. N. Preparation of high-octane oxygenate fuel components from plant-derived polyols. *Pet. Chem.* **2011**, *51* (1), 61−69.

(42) Nanda, M. R.; Yuan, Z.; Qin, W.; Ghaziaskar, H. S.; Poirier, M.-A.; Xu, C. A new continuous-flow process for catalytic conversion of glycerol to oxygenated fuel additive: Catalyst screening. *Appl. Energy* **2014**, *123*, 75−81.

(43) da Silva, C. X. A.; Mota, C. J. A. The influence of impurities on the acid-catalyzed reaction of glycerol with acetone. *Biomass Bioenergy* **2011**, *35* (8), 3547−3551.

(44) Nanda, M. R.; Yuan, Z.; Qin, W.; Ghaziaskar, H. S.; Poirier, M.-A.; Xu, C. C. Thermodynamic and kinetic studies of a catalytic process to convert glycerol into solketal as an oxygenated fuel additive. *Fuel* **2014**, *117* (Part A), 470−477.

(45) Deutsch, J.; Martin, A.; Lieske, H. Investigations on heterogeneously catalysed condensations of glycerol to cyclic acetals. *J. Catal.* **2007**, *245* (2), 428−435.

(46) Esteban, J.; Ladero, M.; García-Ochoa, F. Kinetic modelling of the solventless synthesis of solketal with a sulphonic ion exchange resin. *Chem. Eng. J.* **2015**, *269*, 194−202.

(47) Esteban, J.; Vorholt, A. J.; Behr, A.; Ladero, M.; Garcia-Ochoa, F. Liquid−Liquid Equilibria for the System Acetone+ Solketal+ Glycerol at (303.2, 313.2, and 323.2) K. *J. Chem. Eng. Data* **2014**, *59* (9), 2850−2855.

(48) Faria, R. P. V.; Pereira, C. S. M.; Silva, V. M. T. M.; Loureiro, J. M.; Rodrigues, A. E. Sorption enhanced reactive process for the synthesis of glycerol ethyl acetal. *Chem. Eng. J.* **2014**, *258* (0), 229−239.

(49) Faria, R. P. V.; Pereira, C. S. M.; Silva, V. M. T. M.; Loureiro, J. M.; Rodrigues, A. E. Glycerol valorisation as biofuels: Selection of a suitable solvent for an innovative process for the synthesis of GEA. *Chem. Eng. J.* **2013**, *233* (0), 159−167.

(50) Umar, M.; Saleemi, A. R.; Qaiser, S. Synthesis of ethyl tert-butyl ether with tert-butyl alcohol and ethanol on various ion exchange resin catalysts. *Catal. Commun.* **2008**, *9* (5), 721−727.

(51) Yu, W.; Hidajat, K.; Ray, A. K. Determination of adsorption and kinetic parameters for methyl acetate esterification and hydrolysis reaction catalyzed by Amberlyst 15. *Appl. Catal., A* **2004**, *260* (2), 191−205.

(52) Rac, V.; Rakić, V.; Stošić, D.; Otman, O.; Auroux, A. Hierarchical ZSM-5, Beta and USY zeolites: Acidity assessment by gas and aqueous phase calorimetry and catalytic activity in fructose dehydration reaction. *Microporous Mesoporous Mater.* **2014**, *194*, 126−134.

(53) Silva, V. M. T. M.; Rodrigues, A. E. Kinetic studies in a batch reactor using ion exchange resin catalysts for oxygenates production: Role of mass transfer mechanisms. *Chem. Eng. Sci.* **2006**, *61* (2), 316−331.

(54) Levenspiel, O. *Chemical Reaction Engineering*, 3rd ed.; John Wiley & Sons, Inc.: 1999.

(55) Scheibel, E. G. Correspondence. Liquid Diffusivities. Viscosity of Gases. *Ind. Eng. Chem.* **1954**, *46* (9), 2007−2008.

(56) Perkins, L. R.; Geankoplis, C. J. Molecular diffusion in a ternary liquid system with the diffusing component dilute. *Chem. Eng. Sci.* **1969**, *24* (7), 1035−1042.

(57) Faria, R. P. V.; Pereira, C. S. M.; Silva, V. M. T. M.; Loureiro, J. M.; Rodrigues, A. E. Glycerol valorization as biofuel: thermodynamic and kinetic study of the acetalization of glycerol with acetaldehyde. *Ind. Eng. Chem. Res.* **2013**, *52* (4), 1538−1547.

(58) Nandan, D.; Sreenivasulu, P.; SivakumarKonathala, L. N.; Kumar, M.; Viswanadham, N. Acid functionalized carbon−silica composite and its application for solketal production. *Microporous Mesoporous Mater.* **2013**, *179*, 182−190.

(59) Gandi, G. K.; Silva, V. M. T. M.; Rodrigues, A. E. Process Development for Dimethylacetal Synthesis: Thermodynamics and Reaction Kinetics. *Ind. Eng. Chem. Res.* **2005**, *44* (19), 7287−7297.

(60) Rodrigues, A. E.; Pereira, C. S. M.; Santos, J. C. Chromatographic Reactors. *Chem. Eng. Technol.* **2012**, *35* (7), 1171−1183.

(61) Agirre, I.; García, I.; Requies, J.; Barrio, V. L.; Güemez, M. B.; Cambra, J. F.; Arias, P. L. Glycerol acetals, kinetic study of the reaction between glycerol and formaldehyde. *Biomass Bioenergy* **2011**, *35* (8), 3636−3642.

(62) Agirre, I.; Güemez, M. B.; Ugarte, A.; Requies, J.; Barrio, V. L.; Cambra, J. F.; Arias, P. L. Glycerol acetals as diesel additives: Kinetic study of the reaction between glycerol and acetaldehyde. *Fuel Process. Technol.* **2013**, *116* (0), 182−188.

(63) Güemez, M. B.; Requies, J.; Agirre, I.; Arias, P. L.; Barrio, V. L.; Cambra, J. F. Acetalization reaction between glycerol and n-butyraldehyde using an acidic ion exchange resin. Kinetic modelling. *Chem. Eng. J.* **2013**, *228* (0), 300−307.

(64) Oliveira, P. A.; Souza, R. O.; Mota, C. J. Atmospheric pressure continuous production of solketal from the acid-catalyzed reaction of glycerol with acetone. *J. Braz. Chem. Soc.* **2016**, *27* (10), 1832−1837.